applied sciences

MDPI

Communication

Investigation of Biofabricated Iron Oxide Nanoparticles for Antimicrobial and Anticancer Efficiencies

Nilavukkarasi Mohandoss [1], Sangeetha Renganathan [2], Vijayakumar Subramaniyan [1,*], Punitha Nagarajan [1], Vidhya Elavarasan [1], Prathipkumar Subramaniyan [3] and Sekar Vijayakumar [4,*]

[1] PG and Research Department of Botany, A.V.V.M. Sri Pushpam College, Affiliated to Bharathidasan University, Poondi 613503, India
[2] PG and Research Department of Mathematics, A.V.V.M. Sri Pushpam College, Bharathidasan University, Poondi 613503, India
[3] National Institute of Technology, Tiruchirappalli 620015, India
[4] Marine College, Shandong University, Weihai 264209, China
* Correspondence: svijaya_kumar2579@rediff.com (V.S.); vijaysekar05@gmail.com (S.V.)

Abstract: *Capparis zeylanica* leaf extract was employed in this work to create iron oxide nanoparticles (α-Fe_2O_3) using anhydrous ferric chloride. The UV spectrum, XRD, FT-IR, and FE-SEM with EDX methods were used to characterize the fabricated nanoparticles. The iron oxide nanoparticles obtained were spherical in form, with an average crystallite size of 28.17 nm determined by XRD. The agar well diffusion method was used to assess the antimicrobial activity of the α-Fe_2O_3 nanoparticles created in this study against pathogenic organisms, Gram-negative bacteria (*Escherichia coli* and *Pseudomonas aeroginosa*), Gram-positive bacteria (*Staphylococcus aureus* and *Streptococcus pyogenes*), and fungi (*Candida albicans* and *Aspergillus niger*). Among the pathogens tested, *S. pyogenes* had the highest zones of inhibition (25 $\pm$ 1.26 mm), followed by *S. aureus* (23 $\pm$ 0.8 mm), *E. coli* (23 $\pm$ 2.46 mm), *P. aeroginosa* (22 $\pm$ 1.86 mm), *C. albicans* (19 $\pm$ 2.34 mm) and *A. niger* (17 $\pm$ 3.2 mm). The substance was further tested for anticancer activity against A549 (lung cancer) cells using the MTT assay. The cytotoxic reaction was found to be concentration-dependent. The present study, therefore, came to the conclusion that the bio-effectiveness of the manufactured α-Fe_2O_3 nanoparticles may result in applications in biomedical domains.

Keywords: bio-fabrication; *Capparis zeylanica*; α-Fe_2O_3; antimicrobial activity; lung cancer (A549)

check for updates

Citation: Mohandoss, N.; Renganathan, S.; Subramaniyan, V.; Nagarajan, P.; Elavarasan, V.; Subramaniyan, P.; Vijayakumar, S. Investigation of Biofabricated Iron Oxide Nanoparticles for Antimicrobial and Anticancer Efficiencies. *Appl. Sci.* **2022**, *12*, 12986. https://doi.org/10.3390/app122412986

Academic Editor: Prabakaran Mayakrishnan

Received: 26 November 2022
Accepted: 15 December 2022
Published: 17 December 2022

Publisher's Note: MDPI stays neutral with regard to jurisdictional claims in published maps and institutional affiliations.

Copyright: © 2022 by the authors. Licensee MDPI, Basel, Switzerland. This article is an open access article distributed under the terms and conditions of the Creative Commons Attribution (CC BY) license (https://creativecommons.org/licenses/by/4.0/).

1. Introduction

Nanotechnology has developed a reputation in nanoscience during the past twenty years. Researchers and scientists are actively working to create diverse nanoparticles from innovative materials for various uses [1]. One of the most significant transition metals for biological purposes is iron oxide. Hematite (α-Fe_2O_3) is the most stable polymorph of iron oxide and is ideal for biomedical applications due to its adaptable magnetic and optical characteristics, great chemical stability, and biocompatibility. There are a number of ways to make iron oxide nanoparticles, including mechanochemical methods, wire electrical explosion, electrochemical methods, and green synthesis.

Plants are more favoured than microorganisms as biological resources because of their low cost and simple accessibility in nature. In addition to lowering the metal salt, the biomolecules used in the synthesis also functionalize the nanoparticles' surfaces, leading to synergistic benefits in applications such as cancer therapy or the development of antimicrobial agents [2]. A promising alternative method for creating nanoparticles is through green synthesis. Compared to the currently available, traditional physical and chemical approaches, green synthesis provides a number of benefits [3]. Iron oxides are one of the most biocompatible metal oxide nanoparticles due to their exceptional minuscule physical properties, including superparamagnetism, firmness in liquid solutions, low

susceptibility to oxidation, long blood half-lives, and flexible surface chemistry. They have a wide range of applications in environmental regulation, including as antibacterial drugs, in the adsorption of dyes, in food-related processes, and in the biomedical sector (drug delivery, magnetic cells, immunoassays, and hyperthermia treatment of cancer) [4–11]. In the current work, anhydrous ferric chloride was converted into α-Fe_2O_3 nanoparticles using a *Capparis zeylanica* leaf extract and the nanoparticles were examined for antimicrobial and antiproliferative activities.

2. Materials and Methods

2.1. Materials

$Fecl_3.6H_2O$ of analytical grade was the sole substance employed in the manufacture of the hematite nanoparticles. We bought the bacterial culture medium from HiMedia (Mumbai, India). Sigma Aldrich in the USA provided the ethyl acetate, antibiotic solution, and Dulbecco's Modified Eagle's Medium (DMEM).

2.2. Biosynthesis of α-Fe_2O_3 Nanoparticles

The procedure recommended in prior research [12] was slightly modified to prepare the *C. zeylanica* leaf extract. *C. zeylanica* leaf extract was added to 50 mL of a 0.1 M aqueous solution of ferric chloride hexahydrate along with leaf extract. The orange-coloured ferric chloride hexahydrate solution changed to a brownish-black colour, precipitating a black substance. After being sonicated for 30 min, the mixture was filtered, rinsed with distilled water, and dried. To produce iron oxide nanoparticles, the dried precipitate was heated for three hours at 600 °C in a muffle furnace.

2.3. Characterization of α-Fe_2O_3 Nanoparticles

The X-ray diffraction (XRD) method was used to study the crystallinity of α-Fe_2O_3 nanoparticles. Using a UV–Vis NIR double-beam spectrophotometer, the optical properties of α-Fe_2O_3 was examined at different wavelengths between 300 and 700 nm. The substituents of the nanoparticles were examined using Fourier-transform infrared (FT-IR) spectroscopy (Perkin Elmer RX-I Spectrophotometer). A field emission scanning electron microscope (FE-SEM) was employed to examine the morphology of the α-Fe_2O_3 nanoparticles. The energy-dispersion X-ray (EDX) method was used to analyse the composition of the α-Fe_2O_3 nanoparticles.

2.4. Antimicrobial Activity

The antibacterial activity of the artificial α-Fe_2O_3 nanoparticles was investigated using ethyl acetate-based leaf extracts from *C. zeylanica*. The pathogenic organisms were collected from the Microbial Type Culture Collection (MTCC), Chandigarh, India, and included *Streptococcus pyogenes*, *Staphylococcus aureus*, *Escherichia coli*, *Pseudomonas aeruginosa*, *Candida albicans*, and *Aspergillus niger*. The aforementioned cultures were then cultivated and kept alive at 35 °C for bacterial species and 30 °C for fungal species on Mullar-Hinton agar (MHA) and Sabouraud Dextrose Agar (SDA) media, respectively. In MHA and SDA plates, a 6 mm well was pounded. A micropipette was used to inject 20 µL of sample into each plate's well. Gentamycin (50 µg) served as a positive control for bacteria and fungi. The bacterial and fungal cultures were incubated for 24 h at 30 °C and 72 h at 37 °C, correspondingly. Each experiment was executed three times, with measurements taken in millimetres.

2.5. Anticancer Activity

The National Center for Cell Science (NCCS), Pune, India, provided the lung cancer cell line A549. The cells were cultured in DMEM media supplemented with 10% FBS, Penicillium (100 g/mL), streptomycin (100 g/mL), and amphotericin B (5 g/mL) and incubated overnight. Utilizing the established 3-(4,5-dimethylthiazole-2-yl)-2, 5-diphenyltetrazolium bromide (MTT) tests as described by Chelliah and Oh [13], the cytotoxic impact of syn-

thesized α-Fe_2O_3 nanoparticles on the A549 cell line was assessed. A 96 well plate with 2×10^4 cells per well and a volume of 100 µL was used for cell incubation. After 24 h, the cell layer was treated with various doses (1.45, 3.9, 7.8, 15.6, 31.2, 62.5, 125, 250, 500, and 1000 g/mL) of Fe_2O_3 nanoparticles. Cells were incubated at 37 °C for 4 h after addition of 50 µL of MTT (1 mg/mL) to each well. The development of Formosan crystals was then disrupted in 200 µL of dimethyl sulphoxide after the medium had been withdrawn. A microplate reader was used to measure the absorption over the course of 15 min at a wavelength of 540 nm

2.6. Statistical Analysis

Each test was run in triplicate. One-way variant analysis was performed, and the results are presented as means ± standard errors.

3. Result and Discussion

3.1. UV–Visible Spectrum of α-Fe_2O_3 Nanoparticles

The spectrum of the α-Fe_2O_3 nanoparticles' diffuse reflectance in the UV–visible range is displayed in Figure 1a. The prominent absorption peak at 354 nm corresponds to α-Fe_2O_3 nanoparticles [14].

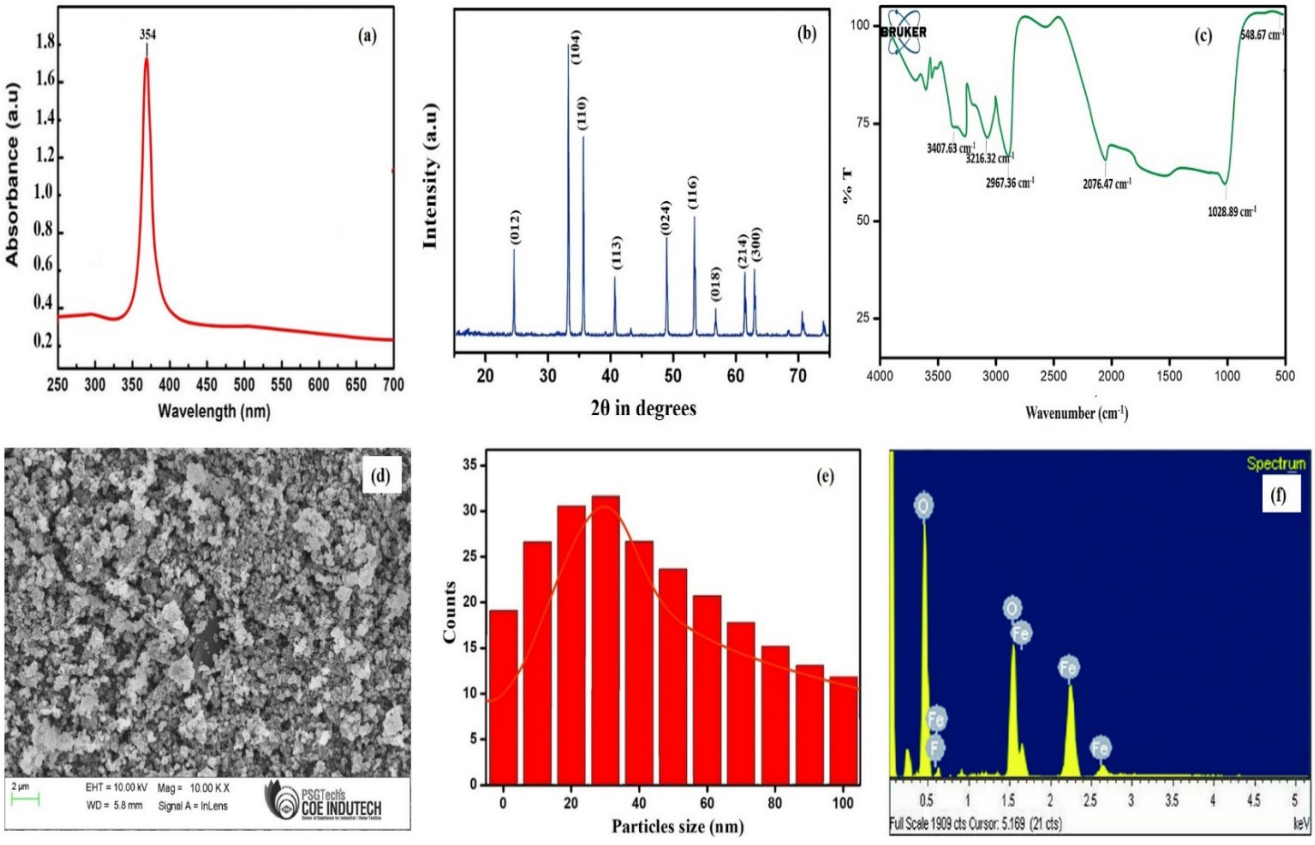


Figure 1. Bio-fabricated α-Fe_2O_3 nanoparticles: (**a**) UV spectrum, (**b**) XRD, (**c**) FT-IR, (**d**) FE-SEM, (**e**) histogram distribution, (**f**) EDAX.

3.2. XRD of α-Fe_2O_3 Nanoparticles

Figure 1b shows the XRD pattern of the α-Fe_2O_3 nanoparticles. The (012), (104), (110), (113), (024), (116), (018), (214), and (300) planes were, respectively, assigned to the XRD peaks at 24.76, 33.52, 35.12, 41.67, 49.79, 54.02, 57.22, 62.52, and 63.82 2h. The wide, sharp peaks further demonstrated the well-crystallized hexagonal structure of the α-Fe_2O_3 nanoparticles (corresponding to JCPDS file no. 33-0664).

3.3. FTIR Spectra of α-Fe_2O_3

The FTIR spectra of α-Fe_2O_3 are shown in Figure 1c. The synthetic α-Fe_2O_3 nanoparticles' infrared spectra (FTIR), which were recorded in the 400–4000 cm^{-1} wavenumber region, were used to identify the compound's chemical bonds and functional groups. The existence of an absorbed water molecule was indicated by the wide band at 3407 cm^{-1}, which was attributed to the O-H stretching vibration [15]. The peaks at 3216 cm^{-1} in the fluoride-treated ferrous oxide-hydroxide nanoparticles were somewhat displaced to lower frequencies, which may have been the result of fluoride adsorption, ion exchange, or both [16]. The bending vibrations of the C-H bond in the organic compounds were thought to be responsible for the absorption peaks at 2967 cm^{-1} [17]. These adsorption peaks at 2076 cm^{-1} for the N=C=S (iso-thiocyanate) group provided evidence that proteins and other bioactive substances were present on the surface of the biosynthesized iron nanoparticles [18]. A small peak at 1028 cm^{-1} was caused by the stretching vibration of C-O H [19]. The FeO_6 octahedron was present in the samples, as seen by the prominent absorption bands at 548 cm^{-1}, which were attributed to the stretching of the Fe-O bond [20].

3.4. FE-SM with EDAX

In Figure 1d, pictures of the synthesized α-Fe_2O_3 nanoparticles obtained using FE-SEM are displayed. The α-Fe_2O_3 nanoparticles in the FE-SEM image are distributed uniformly and have a spherical shape. The α-Fe_2O_3 nanoparticles had an average particle size of 28.17 nm. The fabrication of α-Fe_2O_3 nanoparticles is depicted in Figure 1e as a histogram of the particle size distribution. Figure 1f displays the EDAX pattern. The components that made up the resulting α-Fe_2O_3 nanoparticles were iron (Fe) and oxygen (O).

3.5. Antimicrobial Activity

The substance was tested for its antimicrobial effectiveness against harmful organisms. *Streptococcus pyogenes* exhibited the largest inhibitory zones (25 mm), followed by *Staphylococcus aureus* (23 mm), *Escherichia coli* (23 mm), *Pseudomonas aeroginosa* (22 mm), *Candida albicans* (19 mm), and *Aspergillus niger* (17 mm). With the use of the agar well diffusion technique, a considerable zone of inhibition (ZOI) was discovered, as shown in Figure 2a. Table 1 shows that the rate of microbiological growth decreased as the α-Fe_2O_3 nanoparticle concentration was increased. The results for the synthesized nanoparticles' antimicrobial efficacy against our chosen microorganisms showed that they possessed strong antimicrobial activity.

Similarly, Leisha et al. [21] demonstrated that biosynthesized iron-oxide nanoparticles can inhibit the growth of *Staphylococcus aureus*, *Escherichia coli*, *P. aeruginosa*, and *Streptococcus mutans* and have potential bactericidal activity. The strong antimicrobial activity of the synthesized nanoparticles was likely brought about by the presence of the plant extract on their surfaces. Even though these were extremely positive results, additional research is required to determine whether iron-oxide nanoparticles are a viable alternative to silver nanoparticles for the treatment of bacterial infections. Although the precise mechanism of the antimicrobial action of the α-Fe_3O_4 nanoparticles that causes damage to bacterial proteins and DNA has not yet been identified, it was speculated that it may involve oxidative stress brought about by reactive oxygen species, such superoxide radicals (O_2^-), singlet oxygen ($^1O_2$), hydroxyl radicals (-OH), or hydrogen peroxide (H_2O_2). The process that produces ROS can readily diffuse into the cytoplasm of the cell, causing ROS-induced release in the mitochondria and causing death [22].

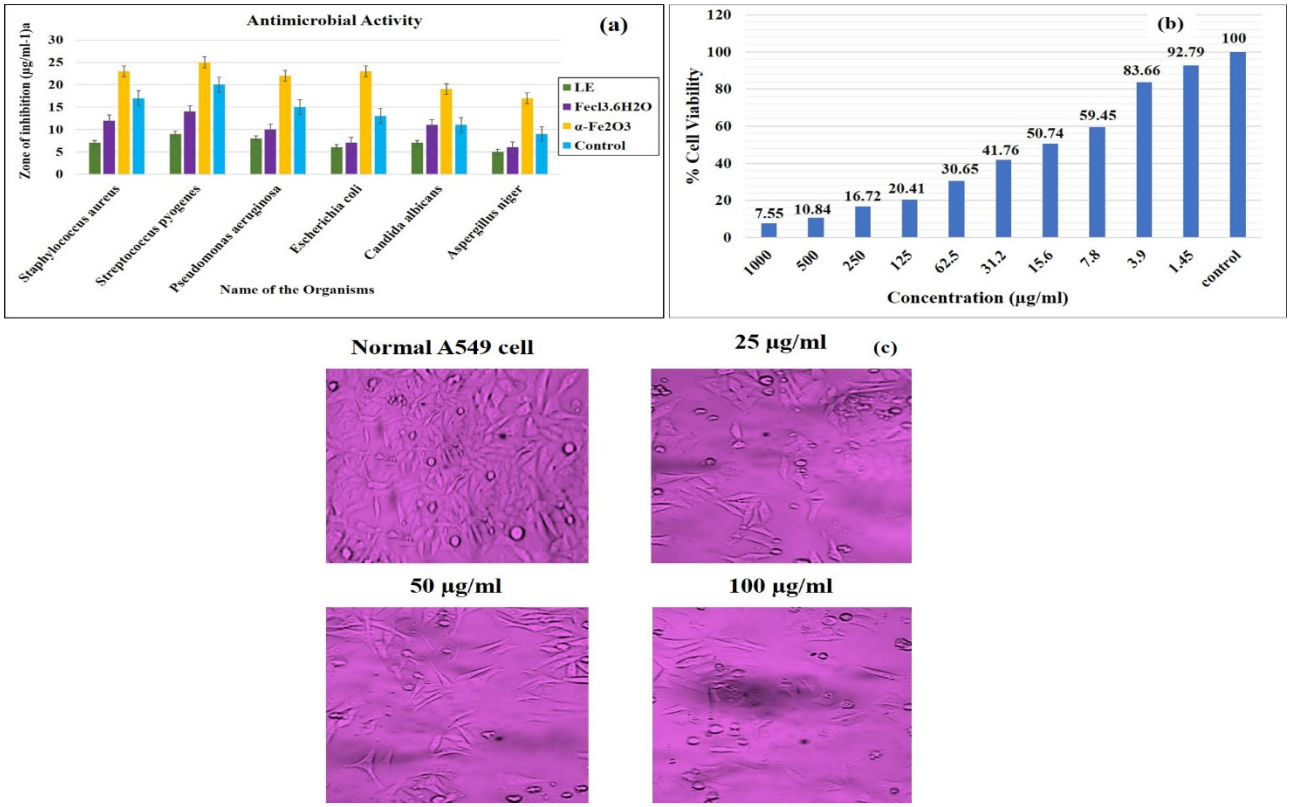


Figure 2. Bio-fabricated α-Fe_2O_3 nanoparticles: (**a**) antimicrobial activity, (**b**) MTT assay, (**c**) anticancer activity.

Table 1. Antimicrobial activity of biosynthesised α-Fe_2O_3 nanoparticles against microorganisms.

S. No.	Name of the Organism	Zone of Inhibition (µg/mL^{-1}) [a]				
		PE	**$Fecl_3.6H_2O$**	**α-Fe_2O_3**	**Positive Control**	**Negative Control**
1.	***Streptococcus pyogenes***	9 ± 1.37	14 ± 1.26	25 ± 2.56	20 ± 1.32	0
2.	***Staphylococcus aureus***	7 ± 1.24	12 ± 1.43	23 ± 2.23	17 ± 1.55	0
4.	***Escherichia coli***	6 ± 0.76	7 ± 0.20	23 ± 1.34	13 ± 1.22	0
3.	***Pseudomonas aeruginosa***	8 ± 1.23	10 ± 1.21	22 ± 1.23	15 ± 1.35	0
5.	***Candida albicans***	7 ± 1.19	11 ± 0.17	19 ± 0.98	11 ± 1.12	0
6.	***Aspergillus niger***	5 ± 0.99	6 ± 1.27	17 ± 1.62	9 ± 0.75	0

[a] Mean values of three triplicates ± standard deviation. **PE**—plant extract, **$Fecl_3.6H_2O$**—ferric chloride hexahydrate, **α-Fe_2O_3**—biosynthesized iron oxide nanoparticles, **Control**—ethyl acetate.

3.6. Anticancer Activity

The α-Fe_2O_3 nanoparticles were tested for cytotoxicity against human A549 cancer cells at a range of doses (1–100 mg/mL). A phase-contrast inverted microscope was used to examine the cell growth. After receiving treatment with α-Fe_2O_3 nanoparticles, A549 cells shrank and their nuclei became fractured and compacted, as shown in the microscopy images in Figure 2b. At lower hematite concentrations (1–10 mg/mL), significant morphological alterations were not seen. According to our research, the substance has a concentration-dependent cytotoxic effect on A549 lung cancer cells (Figure 2c). At a concentration of 15.6 µg/mL, which is regarded as the IC50 value, α-Fe_2O_3 nanoparticles demonstrated 50% cell killing. According to the designated activity levels of the US National Cancer Institute's Center For Cancer Research, the produced nanoparticles are moderately active [23].

4. Conclusions

Biofabricated α-Fe_2O_3 nanoparticles were successfully synthesized using *C. zeylanica* leaf extract. The conformations of the nanoparticles were characterized using various techniques. The α-Fe_2O_3 nanoparticles possess admirable antimicrobial and antiproliferative activities.

Author Contributions: N.M., Methodology; S.R. and P.S., Data curation; P.N., Formal analysis; V.E., Resources; V.S., Writing—Original draft; S.V., Writing—Review and editing. All authors have read and agreed to the published version of the manuscript.

Funding: This research was funded by DST-FIST (SR/FST/College-222/2014) and DBT-STAR (HRD-11011/18/2022-HRD-DBT).

Institutional Review Board Statement: Not applicable.

Informed Consent Statement: Not applicable.

Data Availability Statement: On behalf of all the authors, the corresponding author states that our data are available upon reasonable request.

Acknowledgments: We express our gratitude to the management of A.V.V.M. Sri Pushpam College (Autonomous), Poondi, for providing us with the necessary support and research facilities to complete this work.

Conflicts of Interest: The authors declare no conflict of interest.

References

1. Yusefi, M.; Shameli, K.; Ali, R.R.; Pang, S.W.; Teow, S.Y. Evaluating Anticancer Activity of Plant-Mediated Synthesized Iron Oxide Nanoparticles Using *Punica Granatum* Fruit Peel Extract. *J. Mol. Struct.* **2020**, *1204*, 127539. [CrossRef]
2. Yoonus, J.; Resmi, R.; Beena, B. Evaluation of antibacterial and anticancer activity of green synthesized iron oxide (a-Fe_2O_3) nanoparticles. *Mater. Today Proc.* **2021**, *46*, 2969–2974. [CrossRef]
3. Ahmad, W.; Kumar, J.K.; Amjad, M. Euphorbia herita leaf extract as a reducing agent in a facile green synthesis of iron oxide nanoparticles and antimicrobial activity evaluation. *Inorg. Nano-Met. Chem.* **2020**, *51*, 1147–1154. [CrossRef]
4. Nilavukkarasi, M.; Vijayakumar, S.; Prathip Kumar, S. Biological synthesis and characterization of silver nanoparticles with *Capparis zeylanica* L. leaf extract for potent antimicrobial and anti proliferation efficiency. *Mater. Sci. Energy Technol.* **2020**, *3*, 371–376. [CrossRef]
5. Zununi Vahed, S.; Fathi, N.; Samiei, M.; Maleki Dizaj, S.; Sharifi, S. Targeted Cancer Drug Delivery with Aptamer-Functionalized Polymeric Nanoparticles. *J. Drug Target.* **2019**, *27*, 292–299. [CrossRef] [PubMed]
6. Vasantharaj, S.; Sathiyavimal, S.; Senthilkumar, P.; LewisOscar, F.; Pugazhendhi, A. Biosynthesis of Iron Oxide Nanoparticles Using Leaf Extract of Ruellia Tuberosa: Antimicrobial Properties and Their Applications in Photocatalytic Degradation. *J. Photochem. Photobiol. B Biol.* **2019**, *192*, 74–82. [CrossRef]
7. Vinci, G.; Rapa, M. Noble Metal Nanoparticles Applications: Recent Trends in Food Control. *J. Bioeng.* **2019**, *6*, 10. [CrossRef]
8. Yusof, H.M.; Mohamad, R.; Zaidan, U.H. Microbial Synthesis of Zinc Oxide Nanoparticles and Their Potential Application as an Antimicrobial Agent and a Feed Supplement in Animal Industry: A Review. *J. Anim. Sci. Biotechnol.* **2019**, *10*, 57. [CrossRef]
9. Borah, D.; Das, N.; Das, N.; Bhattacharjee, A.; Sarmah, P.; Ghosh, K. Alga Mediated Facile green Synthesis of Silver Nanoparticles: Photophysical, Catalytic and Antibacterial Activity. *Appl. Organomet. Chem.* **2020**, *34*, e5597. [CrossRef]
10. Hernández, A.A.; Aguirre, G.; Cariño-Cortés, R.; MendozaHuizar, L.H.; Jiménez-Alvarado, R. Iron Oxide Nanoparticles: Synthesis, Functionalization, and Applications in Diagnosis and Treatment of Cancer. *Chem. Pap.* **2020**, *74*, 3809–3824. [CrossRef]
11. Vahidi, H.; Barabadi, H.; Saravanan, M. Emerging Selenium Nanoparticles to Combat Cancer: A Systematic Review. *J. Clust. Sci.* **2020**, *31*, 301–309. [CrossRef]
12. Mughal, B.; Zaidi, S.Z.J.; Zhang, X.; Hassan, S.U. Biogenic Nanoparticles: Synthesis, Characterisation and Applications. *Appl. Sci.* **2021**, *11*, 2598. [CrossRef]
13. Parthasarathy, V.; Selvi, J.; Senthil Kumar, K.P. Evaluation of mechanical, optical and thermal properties of PVA nanocomposites embedded with Fe_2O_3 nanofillers and the investigation of their thermal decomposition characteristics under non-isothermal heating condition. *Polym. Bull.* **2021**, *78*, 2191–2210. [CrossRef]
14. Chelliah, R.; Oh, D.H. Screening for anticancer activity: 3-(4,5-Dimethylthiazol-2-yl)-2,5-diphenyltetrazolium (MTT) assay. In *Methods in Actinobacteriology*; Springer Protocols Handbooks; Dharumadurai, D., Ed.; Humana: New York, NY, USA, 2022; pp. 423–425. [CrossRef]
15. Veeramani, S.; Shanmugam, K.; Sahadevan, R. Folate Targeted Galactomannan Coated Iron Oxide Nanoparticles as a Nanocarrier for Targeted Drug Delivery of Capecitabine. *Int. J. Med. Nano Res.* **2018**, *5*, 25. [CrossRef]

16. Raul, P.K.; Devi, R.R.; Umlong, I.M.; Banerjee, S.; Singh, L.; Purkait, M. Removal of Fluoride from Water Using Iron Oxide-Hydroxide Nanoparticles. *J. Nanosci. Nanotechnol.* **2012**, *12*, 3922–3930. [CrossRef]
17. Si, J.C.; Xing, Y.; Peng, M.L.; Zhang, C.; Buske, N.; Chenbc, C.; Cui, Y.L. Solvothermal synthesis of tunable iron oxide nanorods and their transfer from organic phase to water phase. *CrystEngComm* **2014**, *16*, 512–516. [CrossRef]
18. Gouda, A.R.; Sidkey, N.M.; Shawky, H.A.; Yasser, A.A.H. Biosynthesis, Characterization and Antimicrobial Activity Of Iron Oxide Nanoparticles Synthesized By Fungi. *Al-Azhar J. Pharm. Sci.* **2020**, *62*, 164–179. [CrossRef]
19. Hassan, S.S.M.; Shafy, H.I.A.; Mansour, S.M.M. Removal of pyrene and benzo (a) pyrene micropollutant from water via adsorption by green synthesized iron oxide nanoparticles. *Adv. Nat. Sci. Nanosci. Nanotechnol.* **2018**, *9*, 015006. [CrossRef]
20. Mani, A.D.; Soibam, I. Effect of the Size of the Dopants on the Dielectric and Magnetic Properties of Bi (La,Gd) FeO_3 Multiferroic Materials. *J. Nano Res.* **2018**, *51*, 61–68. [CrossRef]
21. Armijo, L.M.; Wawrzyniec, S.J.; Kopciuch, M. Antibacterial activity of iron oxide, iron nitride, and tobramycin conjugated nanoparticles against *Pseudomonas aeruginosa* biofilms. *J. Nanobiotechnol.* **2020**, *18*, 35. [CrossRef]
22. Rudramurthy, G.R.; Swamy, M.K.; Sinniah, U.R.; Ghasemzadeh, A. Nanoparticles: Alternatives Against Drug-Resistant Pathogenic Microbes. *Molecules* **2016**, *21*, 836. [CrossRef] [PubMed]
23. Chothiphirat, A.; Nittayaboon, K.; Kanokwiroon, K.; Srisawat, T.; Navakanitworaku, R. Anticancer potential of fruit extracts from vatica diospyroides symington type SS and their effect on program cell death of cervical cancer cell lines. *Sci. World J.* **2019**, *9*, 5491904. [CrossRef] [PubMed]